COBEM 2021 26th International Congress of Mechanical Engineering
ABCM Associação Brasileira de Engenharia e Ciências Mecânicas
November 22-26, 2021, Virtual Congress, Brazil

COB-2021-1771
APPLICATION OF TSAI'S THEORY FOR THE DESIGN AND ANALYSIS OF A CARBON/EPOXY STRUCTURE FOR AN ENERGY-EFFICIENCY PROTOTYPE VEHICLE

Eyder Ferreira Augusto
Tecnomin Projetos e Consultoria LTDA, R. Tomé de Souza, 830, Funcionários, Belo Horizonte, 30140-131, MG, Brazil.
eyder.augusto@hotmail.com

Carlos Alberto Cimini Junior
Department of Structural Engineering, Federal University of Minas Gerais, UFMG, Av. Antônio Carlos, 6627, Pampulha, Belo Horizonte, 31270-901, MG, Brazil.
cimini@ufmg.br

Abstract. *The growing public concern about the rising of fossil fuels prices and the emission of pollutant gases, in addition to recent laws that seek to reduce CO_2 emissions, has increased the demand for energy-efficient vehicles. Since the mass of the vehicle has an important impact on its fuel consumption, fiber-reinforced composite materials with high specific stiffness and strength become viable alternatives when compared to the commonly used structural metals, such as steel and aluminum. On the other hand, structural design with composite materials can be expensive and laborious. In the academic environment, energy efficiency competitions such as Shell Eco-Marathon, aim to develop automotive prototypes that can travel a predetermined distance using the least possible amount of fuel. In the current study, the design and analysis of a monocoque structure using a carbon/epoxy composite material system was performed for the prototype of the Milhagem Federal University of Minas Gerais (UFMG) team, aiming at reducing the mass of the vehicle. A novel design approach − Prof. Stephen Tsai's "master ply" method and "unit circle" failure theory − was adopted for both obtaining the properties of the composite material system and designing using maximum strain failure criterion. Deformation and buckling analyzes were performed for different loading conditions for the proposed geometry, respecting the established failure criterion. A reduction of 21.5% in the equivalent mass was obtained in comparison to the previous design of the team, which is compatible with similar studies previously carried out.*

Keywords: composites, design, master ply, unit circle, prototype vehicle, fuel-efficiency

1. INTRODUCTION

The growing public concern about the rising of fossil fuels prices and the emission of pollutant gases, in addition to recent laws that seek to reduce CO_2 emissions, has increased the demand for energy-efficient vehicles (PARK et al., 2015). Since the mass of the vehicle has an important impact on its fuel consumption, the main target of automotive engineering becomes mass reduction without losing performance in terms of speed, handling and comfort (CARELLO et al., 2017).

Therefore, fiber-reinforced composite materials with high specific stiffness and strength become viable alternatives when compared to the commonly used structural metals, such as steel and aluminum (HA; CIMINI JR., 2018). Besides, composite materials also present a high potential for optimization because of their anisotropic nature and the number of design variables, such as fiber orientation in each layer (DUTRA; DE ALMEIDA, 2015).

The use of composite materials, which are widespread in the aeronautical industry (KHANI et al., 2011) and are also present in the aerospace, nautical, military, biomedical and sports industries (DANIEL; ISHAI, 2006), is still uncommon in mass production in the automotive industry (CARELLO; AIRALE; MESSANA, 2014). A concrete example of the impact of the application of composite materials in this area is the Ford LTD vehicle, which had a prototype built in carbon fiber composite so that a direct comparison could be made with the original steel model, what resulted in a 33% reduction in the total mass of the vehicle (BEARDMORE; JOHNSON, 1986).

In the university environment, energy efficiency competitions stand out. The most notorious example is the Shell Eco-Marathon, which aim to develop prototypes that travel a predetermined distance using the least possible amount of fuel (SANTIN et al., 2007). The same way as commercial vehicles, the use of composite materials also results in a high potential for optimization in these prototypes, since their application, in addition to providing high structural performance, also allows the use of complex formats, allowing vehicles to be lighter and with better aerodynamics (MESSANA et al., 2019).

The use of complex geometries, however, leads to the practical need to use finite element analysis to determine the distribution of stresses in the structure and its subsequent optimization (MELO; BI; TSAI, 2017). The use of composite materials, whose mechanical characterization is complex, expensive and time-consuming, also leads to the practical need to reduce the number of mechanical tests (TSAI; MELO, 2016), what makes the usage of "an invariant-based theory of composites" a great alternative to the traditional methods of mechanical characterization (TSAI; MELO, 2016).

Given this scenario, the current study aimed to use the finite element analysis method to perform the structural optimization of the carbon/epoxy composite monocoque of the Milhagem UFMG team prototype, based on "novel design approach" (MELO; BI; TSAI, 2017) in order to reduce the mass of the structure to improve its energy efficiency.

2. STRUCTURAL DESIGN

2.1 Geometry

In order to achieve the Shell Eco-Marathon competition objective of minimizing the prototype's fuel consumption, it is necessary to optimize the vehicle's structure in terms of its weight, while maintaining its resistance (AIRALE; CARELLO; SCATTINA, 2011). Space frame type structures (TSIROGIANNIS et al., 2018) and monocoque type structures (AIRALE; CARELLO; SCATTINA, 2011; CARELLO; AIRALE; MESSANA, 2014; CARELLO; MESSANA, 2015; MESSANA et al., 2019; SANTIN et al., 2007) were studied for this application. The structure of the space frame has its resistance provided by tubes that are mainly loaded in tensile and compression directions (TSIROGIANNIS et al., 2018), while the term "monocoque" refers to a shell-shaped structure that relies entirely on its skins for their capacity to resist loads (MEGSON, 2013).

It is expected that a monocoque has a lower mass compared to a tubular chassis, since the shell structure has a greater potential to increase its stiffness and strength (SANTIN et al., 2007). Its use also has negative implications, among which the need for reinforcement to prevent the buckling effect and support loads external to the plane stands out (CROLLA, 2009). The most used reinforcement in this sense are sandwich structures, bulkheads and stringers.

The monocoque structure presents high torsional rigidity, but it is reduced due to the practical need for openings on the vehicle surface for pilot access and for external visibility (CROLLA, 2009). Therefore, aiming at reducing the vehicle's mass, this was the type of structure used in this study.

In this sense, the monocoque geometry was defined based on CFD analysis for aerodynamic optimization and on the restrictions imposed by Shell Eco-Marathon 2021 rules. The geometries and positions of the windows and the removable part for pilot access (cover) were designed according to the competition's visibility restrictions and seeking to minimize openings in the structure and the consequent reduction in torsional stiffness. Figure 1(a) and Figure 1(b) show, respectively, the exterior and interior components of the CAD model of the monocoque structure.

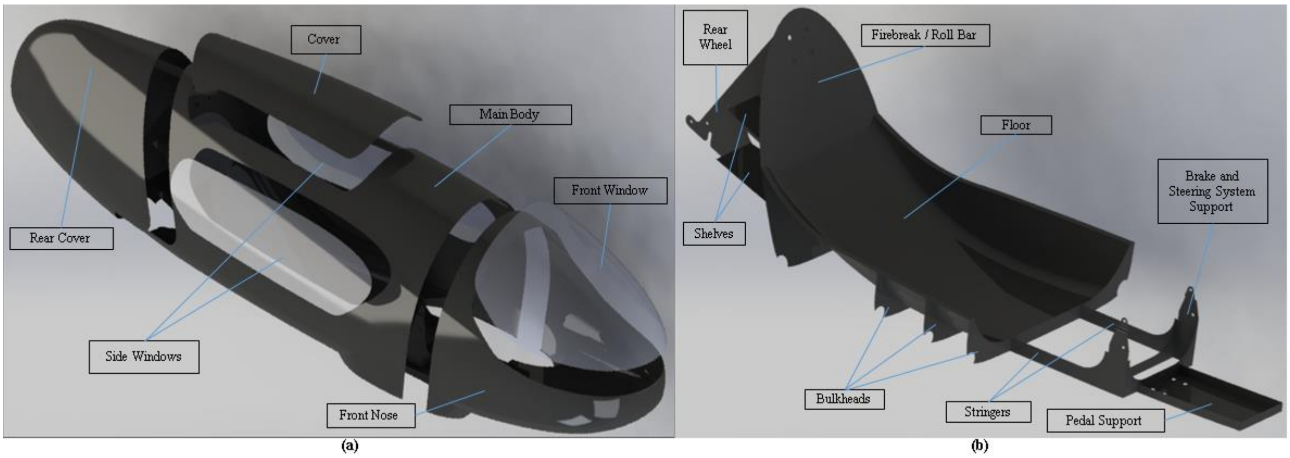

Figure 1. CAD model with all components.

2.2 Materials

Carbon-epoxy composites have high specific stiffness and strength. These characteristics result in a reduction in the weight of components and a consequent reduction in consumption and emissions in vehicles (TSAI; MELO, 2014). Therefore, this type of composite was chosen for the current study. The fabric used was a Tenax® HTS45 E23 3K fiber, 2x2 twill weave and 240g/m^2. The resin used was an ARALDITE® LY1564 BR, manufactured by the company HUNTSMAN®. Therefore, the carbon/epoxy system used is defined as HTS45/LY1564.

Bru et al. (2016) characterized the mechanical properties of an HTS45/LY556 composite system via mechanical tests. This system presents unidirectional reinforcement from the same material and an epoxy matrix from the same manufacturer and mechanical properties similar to the one used in this study (HUNTSMAN®, 2012). As regards to the difference in the shape of the reinforcement, the bidirectional fabric used was treated as a cross-ply laminate $[0/90]_s$ of unidirectional sheets (DANIEL; ISHAI, 2006). Therefore, the values determined by Bru et al. (2016) and presented in Table 1 were used in this study.

Table 1. Mechanical characterization of the HTS45/LY556 unidirectional laminate.

Parameter	**Value**	**Unit**
$E_1^{(1)}$	132	GPa
$E_2^{(1)}$	9.0	GPa
$E_3^{(1)}$	7.3	GPa
G_{23}	Undefined	GPa
$G_{13}^{(2)}$	3.7	GPa
$G_{12}^{(2)}$	4.3	GPa
ν_{12}	0.28	-
ν_{21}	0.029	-
ν_{13}	Undefined	-
ν_{31}	0.02	-
ν_{23}	Undefined	-
ν_{32}	0.43	-
Laminae thickness $^{(3)}$	0.2	mm
Fiber volumetric fraction $^{(3)}$	55	%
Material density $^{(3)}$	1.46	g/cm^3

$^{(1)}$ Lowest value between tension and compression tests
$^{(2)}$ Lowest value between monotonic and cyclic tests
$^{(3)}$ Based on the CP1 $[0/90]_{5s}$ plate

However, due to the high need for reliability of the study and the lack of determination of the values of G_{23}, ν_{13}, and ν_{23}, it was decided to carry out the characterization of the material according to the "master ply". This theory shows that carbon/epoxy composites have common stiffness properties when they are normalized by the trace of their respective stiffness matrix. The median values of these factors after normalization are used to determine a normalized stiffness matrix, called the "master ply" (TSAI; MELO, 2014). Using this theory, it is possible to determine the twelve engineering constants (E_1, E_2, E_3, G_{23}, G_{13}, G_{12}, ν_{12}, ν_{21}, ν_{13}, ν_{31}, ν_{23} and ν_{32}) for a unidirectional carbon/epoxy sheet using only the value of E1 as input data.

Therefore, following the methodology described by Tsai and Melo (2014), Melo, Bi and Tsai (2017) and Cimini Jr. (2020), the trace of the stiffness matrix was determined according to the Eq. (1), in which the value of E_1^* is 0.7351 with a coefficient of variation of 2.9%.

$$Tr[C] = \frac{E_1}{E_1^*} = \frac{132\ MPa}{0.7351} = 179.57\ MPa \tag{1}$$

Then, from the value of Tr[C] and the master ply ([C*]), presented in Eq. (2), the Eq. (3) was used to determine the values of Cij and the stiffness matrix [C], presented in Eq. (4).

$$[C^*] = \begin{bmatrix} 0.7523 & 0.0268 & 0.0268 & 0 & 0 & 0 \\ 0.0268 & 0.0568 & 0.0272 & 0 & 0 & 0 \\ 0.0268 & 0.0272 & 0.0568 & 0 & 0 & 0 \\ 0 & 0 & 0 & 0.0148 & 0 & 0 \\ 0 & 0 & 0 & 0 & 0.0261 & 0 \\ 0 & 0 & 0 & 0 & 0 & 0.0261 \end{bmatrix} \tag{2}$$

$$C_{ij} = C^*_{ij} \,.\, Tr[C] \tag{3}$$

$$[C] = \begin{bmatrix} 135.0886 & 4.8124 & 4.8124 & 0 & 0 & 0 \\ 4.8124 & 10.1994 & 4.8842 & 0 & 0 & 0 \\ 4.8124 & 4.8842 & 10.1994 & 0 & 0 & 0 \\ 0 & 0 & 0 & 2.6576 & 0 & 0 \\ 0 & 0 & 0 & 0 & 4.6867 & 0 \\ 0 & 0 & 0 & 0 & 0 & 4.6867 \end{bmatrix} \quad (4)$$

Once the stiffness matrix [C] was determined, its inverse was calculated in order to determine the compliance matrix [S], shown in Eq. (5).

$$[S] = \begin{bmatrix} 0.0076 & -0.0024 & -0.0024 & 0 & 0 & 0 \\ -0.0024 & 0.1280 & -0.0602 & 0 & 0 & 0 \\ -0.0024 & -0.0602 & 0.1280 & 0 & 0 & 0 \\ 0 & 0 & 0 & 0.3760 & 0 & 0 \\ 0 & 0 & 0 & 0 & 0.2130 & 0 \\ 0 & 0 & 0 & 0 & 0 & 0.2130 \end{bmatrix} \quad (5)$$

Then, the compliance matrix [S] was compared to the general form of the compliance matrix, shown in Eq. (6) in order to determine the 12 engineering constants, which are shown in Table 2.

$$[S] = \begin{bmatrix} 1/E_1 & -\nu_{21}/E_2 & -\nu_{31}/E_3 & 0 & 0 & 0 \\ -\nu_{12}/E_1 & 1/E_2 & -\nu_{32}/E_3 & 0 & 0 & 0 \\ -\nu_{13}/E_1 & -\nu_{23}/E_2 & 1/E_3 & 0 & 0 & 0 \\ 0 & 0 & 0 & 1/G_{23} & 0 & 0 \\ 0 & 0 & 0 & 0 & 1/G_{13} & 0 \\ 0 & 0 & 0 & 0 & 0 & 1/G_{12} \end{bmatrix} \quad (6)$$

Table 2. Mechanical characterization of the HTS45/LY556 unidirectional laminate via "master ply" theory.

Parameter	**Value**	**Unit**
E_1	132	GPa
E_2	7.8	GPa
E_3	7.8	GPa
G_{23}	2.7	GPa
G_{13}	4.7	GPa
G_{12}	4.7	GPa
ν_{12}	0.32	-
ν_{21}	0.02	-
ν_{13}	0.32	-
ν_{31}	0.02	-
ν_{23}	0.47	-
ν_{32}	0.47	-

Finally, the results obtained based on the "master ply" theory were compared with those obtained by Bru et al. (2016). The values obtained from the master ply theory were the ones used, since from it, it is possible to obtain all the necessary values for the mechanical characterization of the material. The values of lamina thickness, fiber volume fraction and material density used followed those determined by Bru et al. (2016). Table 3 presents the parameter values of the laminate used in the finite element analysis.

Table 3. Values of laminate parameters used in finite element analysis.

Parameter	Values			Unit
	Bru et al. (2016)	Master ply	Utilized	
E_1	132	132	132	GPa
E_2	9.0	7.8	7.8	GPa
E_3	7.3	7.8	7.8	GPa
G_{23}	Undefined	2.7	2.7	GPa
G_{13}	3.7	4.7	4.7	GPa
G_{12}	4.3	4.7	4.7	GPa
ν_{12}	0.28	0.32	0.32	-
ν_{21}	0.029	0.02	0.02	-
ν_{13}	Undefined	0.32	0.32	-
ν_{31}	0.02	0.02	0.02	-
ν_{23}	Undefined	0.47	0.47	-
ν_{32}	0.43	0.47	0.47	-
Laminae thickness	0.2	Do not apply	0.2	mm
Fiber volumetric fraction	55	Do not apply	55	%
Material density	1.46	Do not apply	1.46	g/cm^3

The core material used in all sandwich constructions of the monocoque structure, except for the front and rear axle supports, is Coremat® Xi 4, which is a flexible polyester core ideal for manual lamination. The choice to use it was due to the large curvature of the monocoque structure, thus requiring a more flexible core. Table 4 shows the values of the parameters of this material used in the finite element analysis (LANTOR®, 2018), where 20% resin impregnation was considered in the lamination process to calculate the density and estimate the mass.

Table 4. Coremat® Xi 4 parameter values used in finite element analysis.

Parameter	Value	Unit
Elastic modulus (E)	800	MPa
Shear modulus (G)	35	MPa
Thickness	4	mm
Material density	0.15	g/cm^3

ASTM 5052 H32 aluminum alloy plates were used as core material in the sandwich constructions in the front and rear axle supports, which are parts under the major stress. Table 5 presents the parameter values of this material used in the finite element analysis.

Table 5. Parameter values of the ASTM 5052 H32 aluminum alloy used in finite element analysis.

Parameter	Value	Unit
Elastic modulus (E)	70	GPa
Shear modulus (G)	25	GPa
Thickness	15	mm
Material density	2.68	g/cm^3

2.3 Failure criterion

The lamina strength can be characterized by its maximum tensile (F_{1t}, F_{2t} and F_{3t}), compression (F_{1c}, F_{2c} and F_{3c}) and shear strengths (F_{23}, F_{13} and F_{12}) or their corresponding deformations (ε_{1t}, ε_{2t}, ε_{3t}, ε_{1c}, ε_{2c}, ε_{3c}, γ_{23}, γ_{13} and γ_{12}, respectively) (DANIEL; ISHAI, 2006). Commonly used criteria such as Tsai-Wu (TSAI; WU, 1971), Hashin (HASHIN, 1980) and Puck (PUCK; SCHÜRMANN, 1998) use these parameters to determine laminate failure, demanding the performance of mechanical tests to determine these values.

The behavior of the laminate can be described in the strain domain. By controlling the layer in which failure occurs for unit strain vectors with orientation ranging from 0 to 2π, it is possible to determine the domain of strain values for which there is no laminate failure, regardless of the orientation of its plies. This analysis can be done for the failure of the first ply, called "first-ply-failure" or "FPF" (TSAI; MELO, 2014) or for the failure of the last ply, called "last-ply-failure" or "LPF " (TSAI; MELO, 2016). The domain of values for which there is no failure of the last ply of the laminate is shown in Figure 2 and is called “omni strain LPF envelope” (CIMINI JR., 2020).

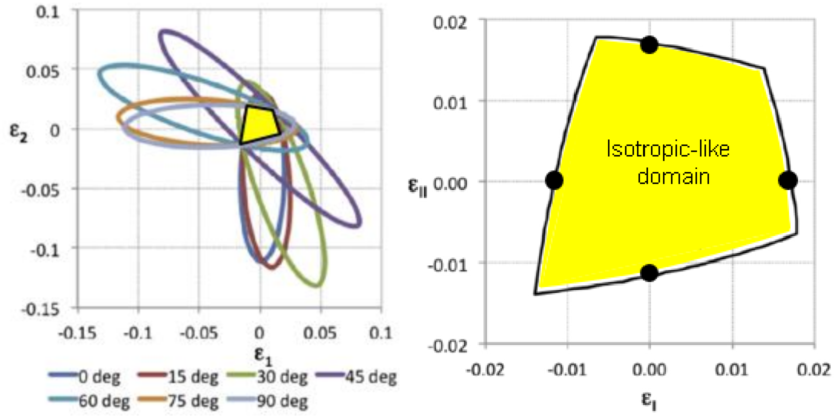

Figure 2. Omni strain LPF envelope.

In this analysis, the inner envelope of LPF is controlled by the plys oriented at 0 and 90° for all carbon fiber reinforced polymer composites. A domain of strain values for which LPF does not occur, called the unit circle failure envelope, can then be established by using only the tensile failure strain (Ɛx) and compression failure strain (Ɛx') values determined from uniaxial mechanical tests (TSAI; MELO, 2016). It is also possible to determine the unit circle failure envelope using only the smallest of values between Ɛx and Ɛx', defining a set of more conservative values (CIMINI JR., 2020)

The criterion currently practiced in the aeronautical industry is the use of a maximum deformation of 0.4% for all epoxy carbon composites (TSAI; MELO, 2014). Called "Nettles' circle", this criterion has the advantage of not requiring the performance of mechanical tests, since it does not use material parameters as input data. This approach presents more conservative results than the analysis via the omni strain LPF envelope and the analysis via the unit circle failure envelope, as shown in Figure 3(CIMINI JR., 2020). For this reason, this was the chosen criterion for the current study.

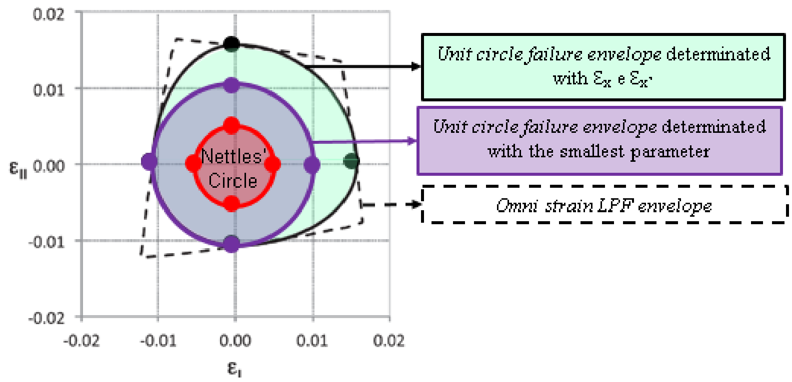

Figure 3. Comparison between omni strain LPF envelope, unit circle and Nettles' circle methods.

2.4 Finite element model

The computational structure modeling procedure using the finite element method consists of four general steps: geometry modeling, domain discretization (mesh creation), specification of material properties and specification of initial, boundary and loading condition (LIU; QUEK, 2003). In this sense, the CAD model was exported to Altair HyperWorks® finite element software, where the HyperMesh® extension was used for pre-processing and mesh generation. First order quadrilateral and triangular 2D shell elements were used on laminated surfaces of the monocoque, as described in item 3.3. The wheels, the steering system, the pedal and the bolted joints were replaced by rigid 1D elements to simplify the model, since these elements are metallic components and were previously analyzed by the Milhagem UFMG team. The average size of the 94703 shell elements used was 5.9 mm, where 2.1% are triangular elements and the greatest curvature deviation was 0.15 mm. Figure 4 shows the mesh used, where the red elements are the 2D shell elements and the gray elements are the rigid elements.

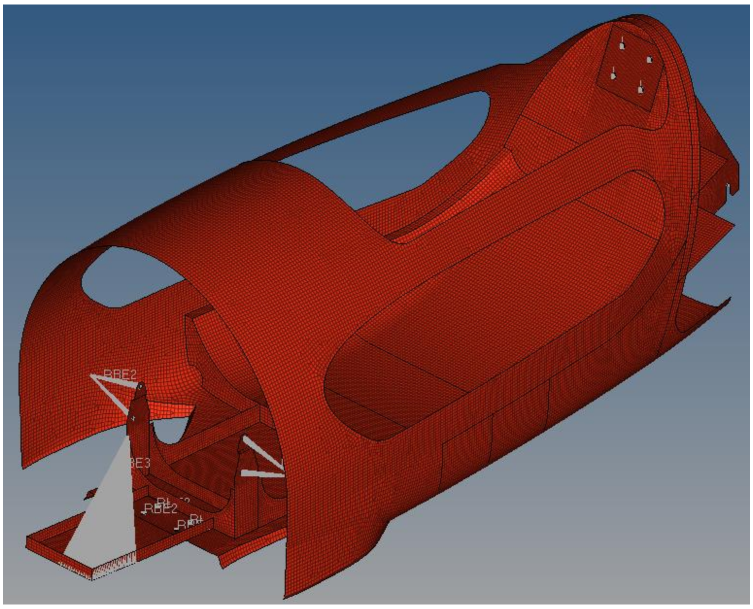

Figure 4. Created mesh.

The acting loads were determined based on the following requirements established in the Shell Eco-Marathon 2021 rules:

• Article 20a: The minimum pilot mass is 50 kg.

• Article 26d: The roll bar must be capable of support a static load of 700 N applied vertically, horizontally and/or perpendicularly, without permanently deforming in any direction.

• Article 42b: Turn radius must be 8 m or less.

• Article 43b: The effectiveness of the braking system will be tested during the vehicle inspection. The vehicle will be placed on a 20% incline with the driver inside. Each brake system will be activated separately, and each individual brake system must hold the vehicle immobile.

In addition, the Milhagem UFMG team provided the following calculation parameters:

• Pilot mass: 55 kg;

• Maximum vehicle speed: 35 km/h or 9.72 m/s;

• Projected turn radius: 7 m;

• Critical braking time: 2.5 s;

• Force applied to the pedal during braking: 400 N.

Then, the acting loads for the different critical load conditions were calculated. These combinations were defined according to previous studies (AIRALE; CARELLO; SCATTINA, 2011; CARELLO; AIRALE; MESSANA, 2014; CARELLO; MESSANA, 2015; MESSANA et al., 2019; SANTIN et al., 2007) and, as in these studies, failure due to fatigue was not verified. This is justified by the fact that these vehicles are subjected to a low number of cycles, due to their low use, and the low loading amplitude, due to good conditions of the track. The loading combinations are described in Table 6.

Table 6. Loads acting in each critical loading condition.

Loading Condition	**Acting Loads**						
	Pilot weight while lying down	**Pilot weight while standing**	**Own weight of the vehicle and its components**	**Centripetal force while cornering**	**Brake force on wheels**	**Brake force on pedal**	**Roll Bar force**
Cornering braking	x		x	x	x	x	
Pilot entrance/exit		x	x				
Vehicle transport			x				
Roll Bar test	x		x				x

3. RESULTS AND DISCUSSION

The Optistruct® extension of the Altair HyperWorks® finite element software was used to solve the analysis and determine the deformations. The final configuration of the laminate is described in Figure 5. The removable parts will be manufactured with laminate $[0/90]_2$.

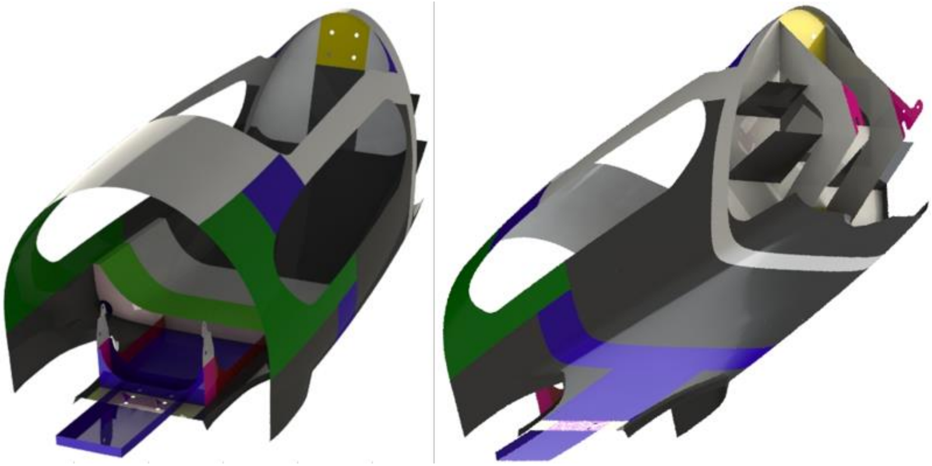

													Bonding of the stringers with the bulkheads and the floor
0°/90°	0°/90°	0°/90°	0°/90°	0°/90°	0°/90°	0°/90°	0°/90°	0°/90°	0°/90°	0°/90°	0°/90°	0°/90°	0°/90°
0°/90°	Coremat	±45°	0°/90°	0°/90°	0°/90°	0°/90°	0°/90°	0°/90°	0°/90°	0°/90°	0°/90°	0°/90°	±45°
	0°/90°	Coremat	Coremat	±45°	0°/90°	0°/90°	0°/90°	0°/90°	0°/90°	0°/90°	0°/90°	0°/90°	0°/90°
		±45°	0°/90°	±45°	0°/90°	0°/90°	0°/90°	0°/90°	0°/90°	0°/90°	0°/90°	0°/90°	±45°
		0°/90°	0°/90°	Coremat	±45°	0°/90°	0°/90°	±45°	0°/90°	0°/90°	0°/90°	0°/90°	0°/90°
				±45°	Coremat	0°/90°	±45°	±45°	±45°	±45°	0°/90°	0°/90°	±45°
				±45°	±45°	Coremat	Coremat	Coremat	±45°	±45°	±45°	0°/90°	0°/90°
				0°/90°	0°/90°	0°/90°	±45°	±45°	Coremat	±45°	±45°	±45°	±45°
				0°/90°	0°/90°	0°/90°	0°/90°	±45°	±45°	±45°	±45°	±45°	0°/90°
					0°/90°	0°/90°	0°/90°	0°/90°	±45°	Coremat	±45°	±45°	±45°
					0°/90°	0°/90°	0°/90°	0°/90°	0°/90°	±45°	±45°	±45°	0°/90°
						0°/90°	0°/90°	0°/90°	0°/90°	±45°	±45°	±45°	±45°
						0°/90°	0°/90°	0°/90°	0°/90°	±45°	5052	±45°	0°/90°
									0°/90°	±45°	±45°	5052	±45°
									0°/90°	0°/90°	±45°	±45°	
										0°/90°	±45°	±45°	
										0°/90°	±45°	±45°	
										0°/90°	±45°	±45°	
										0°/90°	±45°	±45°	
											0°/90°	±45°	
											0°/90°	0°/90°	
											0°/90°	0°/90°	
											0°/90°	0°/90°	
											0°/90°	0°/90°	
												0°/90°	
												0°/90°	
												0°/90°	

Figure 5. Laminate configuration.

The combination that resulted in higher deformation and Von Mises stress values was the pilot entrance/exit, which was also observed in previous studies (AIRALE; CARELLO; SCATTINA, 2011; SANTIN et al., 2007) . The maximum strain and Von Mises stress values were 0.398% and 497MPa, as shown in Figure 6(a) and 6(b), respectively. All combinations led to deformation values lower than 0.4%, respecting the Nettle's circle failure criterion. As regards to Von Mises stress, it was used only as a parameter of comparison, to identify regions of potential stress concentration, and not for failure analysis. In this sense, the use of a quadratic equivalent stress represents the state of stress in the elements with just one parameter.

It is important to emphasize that the highest strain values of the analysis were reached in individual elements of the mesh and occurred due to an unreal stiffness induced by rigid 1D elements used to simplify the model. Figure 6(c) reinforce this statement by presenting the application of a filter in the critical condition of pilot entry/exit. In this filter, only elements with deformations greater than 0.267%, which corresponds to the 0.4% described above divided by a safety factor of 1.5 provided for in the bibliography (YURENKA, 1969), are displayed in color, while elements with deformations lower than this value are presented in grey.

The result of the analysis for the first buckling mode is shown in Figure 6(d). The critical loading condition was cornering braking. The scale magnitude values must be multiplied by the F value to determine the load corresponding to the buckling. Considering that all values of F were negative, for buckling to occur it would be necessary for the loads to act in the opposite direction from the real one. Therefore, it is possible to affirm that the analyzed structure does not fail due to buckling.

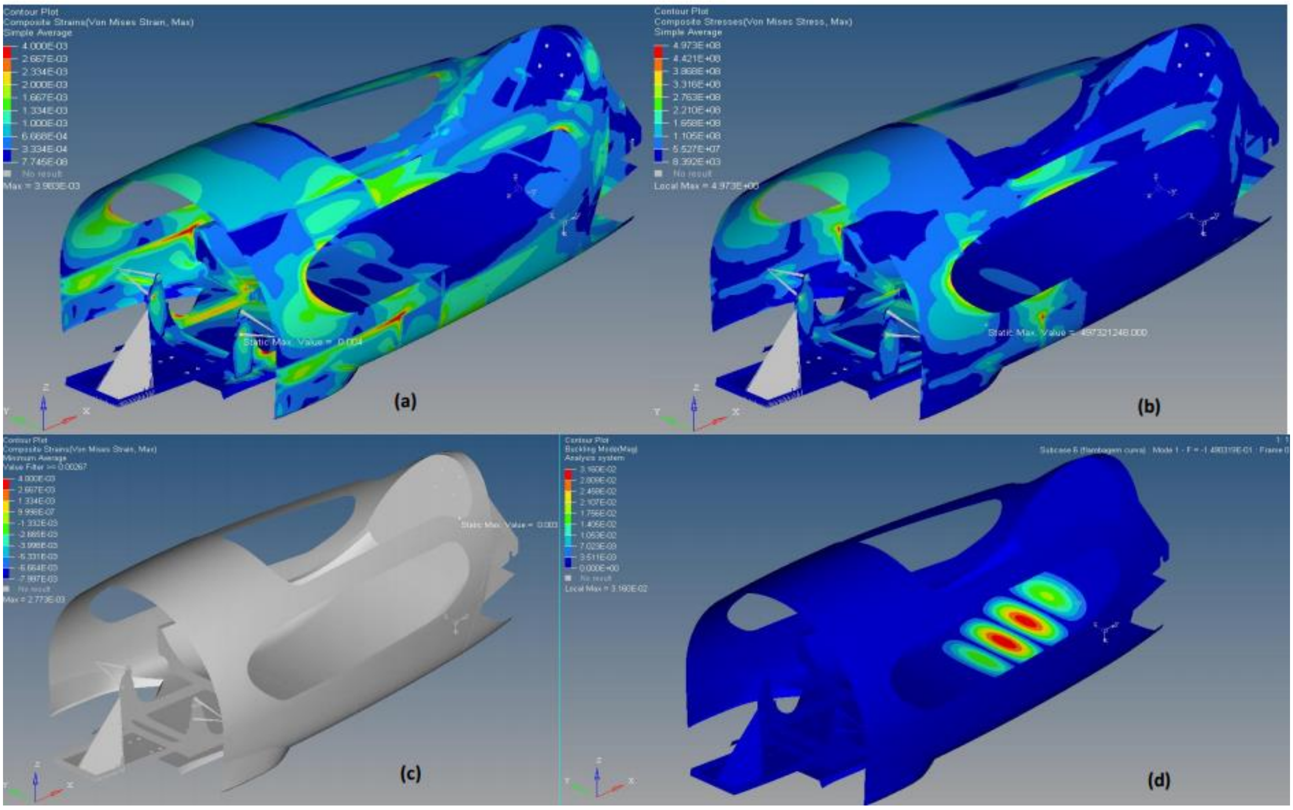

Figure 7. Results of the finite element analysis.

The structure has a projected mass of 10.27 kg for the load-bearing part and 2.67 kg for the removable parts, therefore presenting 12.94 kg of total mass. That represents a reduction of 3.56 kg in comparison to the combined mass of the chassis and fairing of the last Milhagem UFMG prototype (CTM DT1), corresponding to 21.5% of the previous 16.55 kg. The value obtained is similar to the mass of 11.2 kg reported by Messana et al. (2019), especially considering that, opposing to the current study, this value does not take into account the support of the brake and steering system, the support of the rear wheel, the floor and the trays for positioning the electronic components. Carello, Airale and Messana (2014) reported a mass of 6.5 kg for the outer shell of the main body and do not inform the mass of the other components, therefore making difficult a direct comparison with the current study.

4. CONCLUSIONS

The carbon/epoxy composite was proven the most suitable material for application in the current study when compared to conventional materials, such as steel and aluminum, and with other composite materials. In addition, the monocoque-type structure was proven the most suitable for application in the current study when compared to the space frame-type structure.

The Nettles' circle failure criterion was proven the most suitable for application in the current study when compared with other failure criteria analyzed. The values of the properties of the carbon/epoxy composite used were considered as a conservative approximation of the real values, since the lowest values between the bibliography and the calculation using the master ply method were used.

The loading conditions considered were in accordance with the Shell Eco-Marathon rules and with the bibliography and the projected geometry is in accordance with the Shell Eco-Marathon rules.

The entire structure was in accordance the established failure criterion and it does not fail due to buckling, since it would be necessary for the loads to act in the opposite direction from the real one. The mass values obtained were in accordance with the bibliography, presenting a reduction of 21.5% in the corresponding mass in relation to the previous prototype of the Milhagem UFMG team.

The main limitation of the current study was its performance during the COVID-19 pandemic period, which limited access to UFMG facilities. Therefore, it was not possible to carry out mechanical tests to determine the material properties or to validate the finite element model more accurately. For that reason, it is proposed to carry out these tests in future studies. In addition, a subsequent step to the structural analysis is the project and the manufacture of molds and components. Therefore, the description of these processes is also proposed for future studies.

5. REFERENCES

AIRALE, A.; CARELLO, M.; SCATTINA, A. Carbon fiber monocoque for a hydrogen prototype for low consumption challenge. Materialwissenschaft und Werkstofftechnik, v. 42, 2011.

BEARDMORE, P.; JOHNSON, C. F. The potential for composites in structural automotive applications. Composites Science and Technology, v. 26, n. 4, p. 251–281, 1986.

BRU, T. et al. Characterisation of the mechanical and fracture properties of a uni-weave carbon fibre/epoxy non-crimp fabric composite. Data in Brief, v. 6, p. 680–695, 2016.

CARELLO, M. et al. Static Design and Finite Element Analysis of Innovative CFRP Transverse Leaf Spring. Applied Composite Materials, v. 24, 2017.

CARELLO, M.; AIRALE, A.; MESSANA, A. IDRApegasus: A carbon fiber monocoque vehicle prototype. Materialwissenschaft und Werkstofftechnik, v. 45, 2014.

CARELLO, M.; MESSANA, A. IDRA pegasus : a fuel-cell prototype for 3000 km/L. Computer-Aided Design and Applications, v. 12, p. 1–11, 2015.

CIMINI JR., C. A. 36TH INTERNATIONAL CAE CONFERENCE AND EXHIBITION. Simplifying carbon/epoxy composite laminate design. Anais...Evento virtual: 2020

CROLLA, D. A. Automotive Engineering: Powertrain, Chassis System and Vehicle Body. 1. ed. Oxford: Elsevier Inc., 2009.

DANIEL, I. M.; ISHAI, O. Engineering Mechanics of Composite Materials. 2. ed. Nova York: Oxford University Press, 2006.

DUTRA, T. A.; DE ALMEIDA, S. F. M. Composite plate stiffness multicriteria optimization using lamination parameters. Composite Structures, v. 133, p. 166–177, 2015.

HA, S. K.; CIMINI JR., C. A. Theory and validation of the master ply concept for invariant-based stiffness of composites. Journal of Composite Materials, v. 52, n. 12, p. 1699–1708, 2018.

HASHIN, Z. Failure Criteria for Unidirectional Fiber Composites. Journal of Applied Mechanics, v. 47, n. 2, p. 329–334, 1980.

HUNTSMAN®. Composite Resins Selector Guide. Disponível em: <https://pdf.directindustry.com/pdf/huntsman-advanced-materials/composite-resins-selector-guide/26548-330133.html>. Acesso em: 29 jan. 2021.

KHANI, A. et al. Design of variable stiffness panels for maximum strength using lamination parameters. Composites Part B: Engineering, v. 42, n. 3, p. 546–552, 2011.

LANTOR®. Core Below the Waterline. Disponível em: <http://feiplar.com.br/pos_feira/apresentacoes/dia06/nautico/painel_nautico_landor.pdf>. Acesso em: 30 jan. 2021.

LIU, G. R.; QUEK, S. S. The Finite Element Method: A Practical Course. 1. ed. Oxford: Butterworth-Heinemann, 2003.

MEGSON, T. H. G. Aircraft Structures for engineering students. 5. ed. Oxford: Elsevier Ltd., 2013.

MELO, J. D. D.; BI, J.; TSAI, S. W. A novel invariant-based design approach to carbon fiber reinforced laminates. Composite Structures, v. 159, p. 44–52, 2017.

MESSANA, A. et al. From Design to Manufacture of a Carbon Fiber Monocoque for a Three-Wheeler Vehicle Prototype. Materials, v. 12, p. 332, 2019.

PARK, J. et al. Light-weight design of automotive suspension link based on design of experiment. International Journal of Automotive Technology, v. 16, p. 67–71, 2015.

PUCK, A.; SCHÜRMANN, H. Failure analysis of FRP laminates by means of physically based phenomenological models. Composites Science and Technology, v. 58, n. 7, p. 1045–1067, 1998.

SANTIN, J. J. et al. The world's most famous fuel efficiency vehicle – Design and Development of Pac-Car II. Zurique: vdf Hochschulverlag AG, 2007.

TSAI, S. W.; MELO, J. An Invariant-Based Theory of Composites. Composites Science and Technology, v. 100, 2014.

TSAI, S. W.; MELO, J. D. D. A unit circle failure criterion for carbon fiber reinforced polymer composites. Composites Science and Technology, v. 123, p. 71–78, 2016.

TSAI, S. W.; WU, E. M. A General Theory of Strength for Anisotropic Materials. Journal of Composite Materials, v. 5, n. 1, p. 58–80, 1971.

TSIROGIANNIS, E. et al. Lightweight Design and Welding Manufacturing of a Hydrogen Fuel Cell Powered Car's Chassis. Challenges, v. 9, p. 25–40, 2018.

YURENKA, S. (ED.). Composite Materials: Testing and Design. West Conshohocken, PA: ASTM International, 1969.

6. RESPONSIBILITY NOTICE

The authors are the only responsible for the printed material included in this paper.